IEEE Access
Multidisciplinary | Rapid Review | Open Access Journal

Received December 19, 2017, accepted February 7, 2018, date of publication February 14, 2018, date of current version March 12, 2018.

Digital Object Identifier 10.1109/ACCESS.2018.2805940

Reignition After Interruption of Intermediate-Frequency Vacuum Arc in Aircraft Power System

JIANG YUAN, (Member, IEEE), WU JIANWEN, (Member, IEEE), AND JIA BOWEN
School of Automation Science and Electrical Engineering, Beihang University, Beijing 100191, China

Corresponding author: Wu Jianwen (wujianwen@buaa.edu.cn)

This work was supported in part by the National Natural Science Foundation of China under Grant 51377007, in part by the Specialized Research Fund for the Doctoral Program of Higher Education under Grant 20131102130006, and in part by the Fundamental Research Funds for the Central Universities.

ABSTRACT Intermediate frequency (IF) electric power supply system has been widely applied in airplanes. Reignition after interruption of 360–850 Hz vacuum arc in axial magnetic field (AMF) is studied in this paper. According to the experimental results, the current interruption ability decreases from 22.4 kA at 360 Hz to 14.0 kA at 850 Hz. With the increase of frequency, the rate of change of current, di/dt, at current zero (CZ) reaches the breaking threshold at a smaller current value. Based on the least squares solution of the Mayr model, the time of decay of arc energy is prolonged when interruption fails, which is disadvantageous to the breaking process. On the other hand, the eddy effect is enhanced by higher frequency, which increases the residual magnetic induction intensity and the hysteresis phase of AMF after CZ. As a result, the diffusion of plasma is blocked. In the experiments, we find that the position of arc reignition always appears at the margin of contacts. It is shown by calculation that the electric field at the marginal area is twice as strong as that inside the contact. The current density is high, where the electric field is strong, leading to the higher probability of field emission. Arc images are analyzed by frame differential method. The sputtering velocity of macroscopic particles is estimated to be 10–20 m/s. The dissipation time of the macroscopic particles is longer than the arc time of IF vacuum arc, and the presence of macroscopic particles leads to the arc reignition. The findings of this paper would be beneficial to the parameter design of IF vacuum circuit breakers, such as the magnetic flux density of AMF, the chamfering of contact margin, and contact materials.

INDEX TERMS Aircraft, dielectric recovery strength, eddy current effect, intermediate frequency vacuum arc, macroscopic particles, marginal effect of electric field.

I. INTRODUCTION

In some more-electric aircrafts, electricity is generated by a frequency-varying generator and the current frequency is in the range of 360-800 Hz, which is called intermediate frequency (IF) power supply system. As the frequency and current increase, the interruption process becomes difficult and hence new circuit breakers are required to ensure the safety of the aircraft. Vacuum circuit breakers have been widely used in medium/low voltage power systems, and are potentially suitable for use in the IF power supply system in aircrafts. In the field of research on vacuum arc in the aviation IF power supply system, Wang analyzed vacuum arc at 360-800 Hz in an axial magnetic field (AMF) vacuum interrupter with 66 mm diameter. The relationship between arc properties, such as arc shape, current interruption ability, arc voltage noise, anode melting phenomenon, and current frequency was discussed [1], [2]. Zhu studied the vacuum arc motion characteristics at 360-800 Hz in a transverse magnetic field (TMF). The arc would move only when the current increased to a certain value. If the cathode surface was occupied by cathode spots, there would be high frequency noise in the arc voltage [3]–[5]. Jiang considered that the contacts material played a key role in determining the breaking capacity of the vacuum interrupters and the characteristics of an IF vacuum arc. When the current fails to be interrupted, the arcs overflow the gap and exhibit irregular performances in the first half wave [6].

The success of the interruption is determined by the competition between the rise rate of recovery voltage (RRRV) and the recovery rate of dielectric strength (RRDS). If RRDS

is less than RRRV, the arc will reignite after extinguishing [7], [8]. In high current mode, a sharp increase in input power will cause the rate of melting of anode material to increase, which contributes to evaporation of metals and sputtering of macroscopic particles. The dielectric strength will be reduced by a large amount of metal vapors and particles [9], [10]. Densities and spatiotemporal distributions of copper vapor particles in vacuum arc have been measured using laser-induced fluorescence [11], [12]. Wantanabe estimated the anode surface temperature of CuCr50, and the critical vapor density and pressure at the current interruption limit. It was concluded that the reignition might be mainly dominated by the vapor density in the gap [13]. Researchers also found various kinds of copper particles at macroscopic level in the arc column and liquid copper formed a clockwise swirl flow on the contact plate in AMF, which led to interruption failure. In the process of vacuum arc breaking, the energy injected into the anode will cause anode melting, evaporation, and deformation. The arc contraction will lead to more serious anode deformation and the deformation also can influence the dielectric recovery process significantly [14], [15]. Qin investigated the dielectric recovery strength influenced by 375-1000 Hz reverse current in a DC interrupting process. It was found that decreasing the frequency of the reverse current can improve the dielectric recovery strength [16].

Thus, many scholars have tried to explain arc reignition phenomenon and study the cause of the RRDS, however there is not a unified explanation for vacuum arc interruption failure. In addition, most of the existing recent researches are aimed at the power frequency arc, while the research on the vacuum arc at intermediate-frequency is in the initial stage. In this study, interruption experiments of vacuum arc at 360-850 Hz are carried out and the reignition phenomenon is investigated. From the rate of change of current di/dt, the arc energy and the hysteresis of AMF at current zero (CZ), we explain the reason why the current interruption ability decreases with the increase in frequency. The influence of marginal effect on field emission and reignition location are analyzed. Based on the results, the process of arc reignition seems to be impacted by macroscopic particles.

II. EXPERIMENTAL CONDITIONS

The experimental system for IF vacuum arc is shown in Fig. 1. The oscillating circuit which consists of a capacitance C_1, inductance L_1, TRIAC T_1, and vacuum circuit breaker (VCB), is used to generate an oscillating current at 360-850 Hz. The arc branch consists of an electrolytic capacitor C_2, power diode D_1, current-limiting resistor R_2, and SCR T_2, whose function is to make an approximate DC arc in VCB until the oscillating current is injected. The frequency regulation branch is composed of R_0 and C_0, which can adjust the rate of the recovery voltage du/dt after CZ. The current is measured by shunt R_1 with a 0.6 mΩ resistance.

The trigger signal for each branch is controlled by the trigger and recording system and the action sequence in the experiment is as follows. After C_1 and C_2 have been full

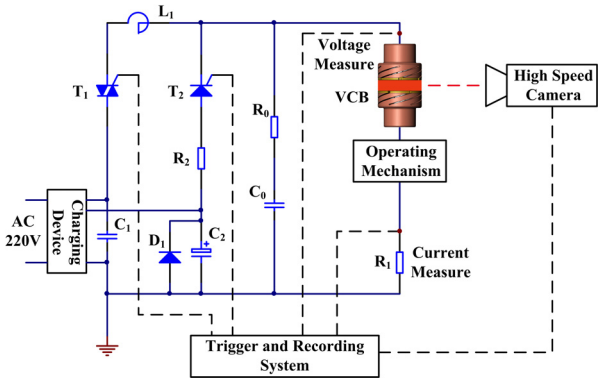

FIGURE 1. Experimental system for 360-850 Hz vacuum arc.

charged, T_2 is triggered when the VCB is closed. Next, the VCB is opened by the operating mechanism and an approximate DC arc is generated. When the VCB opens to the rated separation, the high-speed camera is triggered. Then T_1 is triggered, injecting the IF oscillating current. T_2 will be switched off by a reverse voltage if T_1 is switched on because the charging voltage of C_1 is higher than that of C_2. T_1 is not switched off until the end of the experiment.

In the experiment, a DL750 waveform recorder (YOKOGAWA) is used to record the voltage and current. The maximum recovery voltage is about 500 V and the limit value of the voltage probe is 2000 V. A Phantom v7.3 high speed camera is used to capture the arc images at a sampling rate of 35,087 and a resolution of 320 $\times$ 240.

III. RESULTS AND DISCUSSION

A. INTERRUPTION ABILITY RELATED TO FREQUENCY

Interruption ability for short circuit current is one of the important parameters of vacuum interrupter. In order to study the limit interruption ability at different frequencies and analyze the main factors affecting its open circuit performance, VCB of AMF type with contact materials of CuCr50 and diameter of 41 mm is tested in this section, with a contact distance of 3 mm. By changing the current frequency, we obtain the current peak value in the first half wave for successful and failed interruption at different frequencies, as shown in TABLE 1, represented by I_{success} and I_{failure} respectively. For each frequency, the limit interruption test is performed more than 15 times. It should be noted that when the current frequency is 500 Hz and current peak is 16.5 kA, breaking is sometimes successful and sometimes fails. Therefore, we consider 16.5 kA at 500 Hz as a critical value and 15.5 kA at 600 Hz also as a critical value for the same reason.

As shown in Fig. 2, I_{success} and I_{failure} at different frequencies are represented by curves with symbol $\circ$ and $\times$, respectively; then the limit interruption current must be between the curves $\circ$ and $\times$. We can conclude that with the increase of frequency, the limit breaking ability of AMF type vacuum interrupter decreases. From the macroscopic aspect,

TABLE 1. Current level for successful and failed interruption at different frequency (AMF, CuCr50, 41 mm).

f [Hz]	$I_{success}$ [kA]	$I_{failure}$ [kA]
360	19.9	22.4
500	16.5	16.5
600	15.5	15.5
680	14.4	15.0
850	13.3	14.0

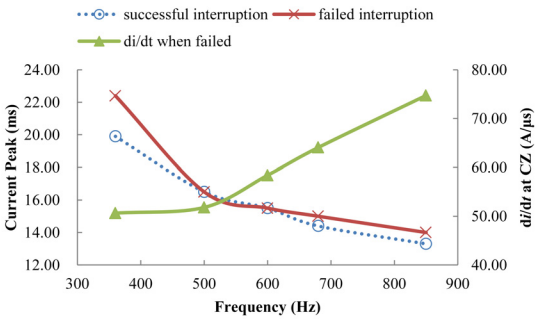

FIGURE 2. Limit interruption ability at different frequencies (AMF, CuCr50, 41 mm).

the interruption process is determined by the competition between the RRRV and RRDS. The RRDS is affected by many factors, such as the di/dt at CZ, the hysteresis of the AMF, the thermal state of the contact, etc. Because the RRRV du/dt, which is determined by R_0 and C_0 in Fig. 1, is constant at different frequencies, we will pay attention to the di/dt at CZ, the arc energy and the hysteresis of the AMF in this paper.

As shown in Fig. 2, di/dt of CZ at different frequencies under failed interruption are represented by the curve. The di/dt increases from about 50 A/μs at 360 Hz to 75 A/μs at 850 Hz. Because the di/dt reaches a maximum at CZ, it is related to the frequency and current peak as,

$$\left.\frac{\mathrm{d}i}{\mathrm{d}t}\right|_{\max} = \left.\frac{\mathrm{d}\left[I_{\mathrm{peak}}\sin(2\pi f\cdot t)\right]}{\mathrm{d}t}\right|_{t=0} = 2\pi f\cdot I_{\mathrm{peak}} \quad (1)$$

The above equation illustrates that with a higher frequency, a smaller current value will cause the same di/dt. If it is considered that there is a threshold of di/dt in VCB, then it will be more difficult to break with the increase in frequency.

According to the Bennet pinch model, the pressure difference between the inside and the edge of the arc column is,

$$\Delta P(r) = \mu_0 \int_r^{r_h} \left(\frac{J_r}{r}\int_0^r J_r \mathrm{d}r\right)\mathrm{d}r \quad (2)$$

Due to the skin effect, with the increase of the current rate, the distribution density of current, Jr, will be high at the center and low at the edge of the arc column, as a result of which the arc pressure at the column center increases and the constriction of the arc will be more apparent [17]. The above phenomenon can be observed in Fig. 8, which shows the arc images of failure interruption at different frequencies. The heat and the energy density are high due to the contraction of the arc, which will enhance the stability of the arc. Then, when the current decreases to zero, the number of cathode spots and plasma will decrease slowly, caused by the high current rate di/dt. There will be residual current in the arc area at CZ, which weakens the dielectric recovery strength. So, the interruption at 850 Hz is worse than that at 360 Hz.

According to the Mayr model, the differential equation for an arc is,

$$g'(t) = \frac{\mathrm{d}g(t)}{\mathrm{d}t} = \frac{g(t)}{\tau}\left(\frac{u(t)\cdot i(t)}{P_0} - 1\right) \quad (3)$$

In this case, $g(t)$ is the conduction of arc, $u(t)$ is the arc voltage, and $i(t)$ is the current. P_0 is the heat dissipation power of arc, and τ is the time constant of arc. To solve for P_0 and τ, we need to obtain the least squares solution of equation (4),

$$\min J(\tau, P_0) = \min \sum_{i=1}^{N} [g'(t_i) - (\frac{1}{\tau P_0} g(t)\cdot u(t)\cdot i(t) - \frac{1}{\tau} g(t))]^2 \quad (4)$$

Based on the arc voltage and current data in the experiment, we can calculate the heat dissipation power and the time constant of arc at various current and frequency conditions, as shown in TABLE 2. The experimental data for failed interruption is indicated in a bold, italic font.

TABLE 2. Heat dissipation power and time constant of arc.

f [Hz]	I [kA]	P_0 [kW]	τ [μs]
360	10.0	247.18	48.05
360	14.0	361.07	68.88
360	19.9	653.80	50.54
360	***22.4***	***875.02***	***73.35***
500	15.0	471.32	19.06
500	16.5	539.45	2.00
500	***16.5***	***549.93***	41.72
600	14.0	421.33	10.32
600	15.5	510.67	3.95
600	***15.5***	***508.90***	***38.26***
680	14.4	446.04	1.66
680	***15.0***	***516.56***	***36.02***
850	13.3	535.79	7.02
850	***14.0***	***521.02***	***40.83***

According to the data in the table, the order of magnitudes of P_0 and τ are consistent in different experimental conditions, indicating that the results are reliable. The effect of the current on P_0 is obvious, and P_0 increases with the increase of the breaking current, as shown in Fig. 3 (a). This is because an increase in current implies an increase in the input power of arc. Then, to ensure a power balance, the heat dissipation power will be increased. The variation of the time constant of arc is more complicated. On the macro level, the time constant of arc at 360 Hz is larger than that at other

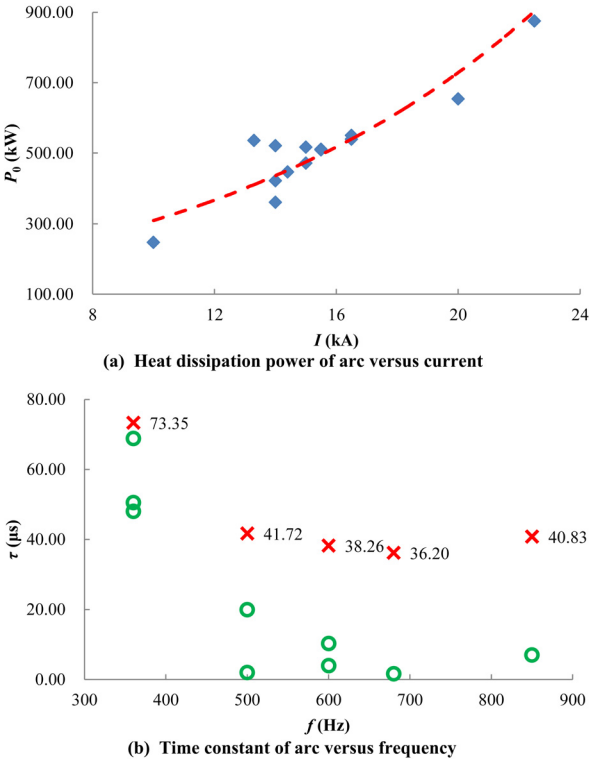

FIGURE 3. Parameters of the Mayr model.

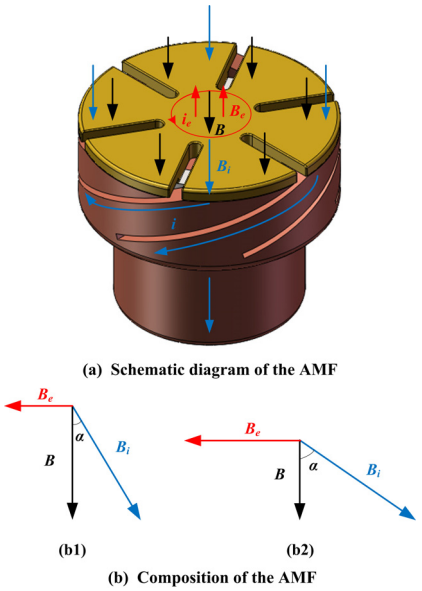

FIGURE 4. The AMF generated by the contacts.

frequencies, indicating that the arc time affects τ. At the same frequency, the time constant increased significantly in the failed interruption, as shown in Fig. 3 (b), in which successful interruption is presented by the symbol ∘, and failed interruption is presented by the symbol ×. This means that the arc energy decays slowly when a failed interruption occurs, which is disadvantageous for the break.

B. HYSTERESIS OF THE AMF

On the other hand, as the current frequency increases, the eddy current effect of the AMF will be stronger, causing the hysteresis of AMF more strongly. The AMF, $\boldsymbol{B}$, in the contact gap is related to the current magnetic field, $\boldsymbol{B_i}$, generated by the current, i, and eddy current magnetic field, $\boldsymbol{B_e}$, generated by the eddy current, i_e, as illustrated in Fig. 4 (a).

According to the Ampere circuital theorem and Faraday's law of electromagnetic induction,

$$\oint_l \boldsymbol{B} \cdot \mathrm{d}\boldsymbol{l} = \mu_0 I \tag{5}$$

$$e = -\frac{d\Phi}{dt} \tag{6}$$

As known from equations (5) and (6), the current, i, which flows through the contacts, is in the same phase as the current magnetic field, $\boldsymbol{B_i}$. The eddy current, i_e, is inducted by AMF and the eddy current magnetic field, $\boldsymbol{B_e}$, lags behind B by 90°. The composition of the AMF is shown in Fig. 4 (b), in which the angle, α, indicates the phase by which the current magnetic field, $\boldsymbol{B_i}$, lags behind the AMF, $\boldsymbol{B}$.

While the current frequency is constant and the amplitude increases, $\boldsymbol{B_i}$ and $\boldsymbol{B_e}$ will increase in proportion; thus the hysteresis phase, α, is constant. However, if the current amplitude is constant and the frequency increases, the amplitude of $\boldsymbol{B_i}$ is constant and the amplitude of $\boldsymbol{B_e}$ increases. To maintain a vector synthesis relationship, the amplitude of $\boldsymbol{B}$ must decrease, as well as the hysteresis phase α must increase, as displayed in Fig. 4 (b). Therefore, the eddy current effect and the hysteresis phenomenon will be strengthened by the increase of frequency. Moreover, the hysteresis of AMF after CZ is also an important factor affecting reignition and breaking ability. With regard to the vacuum arc at power frequency, Wang has simulated delay time of the AMF type contact. It is found that the maximum delay time is not more than 0.6 ms at the contact center [18]. As the cycle time is changed with variation in frequency, the delay time is not sufficient to explain the problem. So, we introduce current phase, θ, to analyze the magnetic properties at different frequencies. For example, θ is 90° at the peak current. The current is given by

$$i(\theta) = I_{\text{peak}} \sin(2\pi f \cdot t) = I_{\text{peak}} \sin\theta \tag{7}$$

where I_{peak} is the current peak, f is the frequency and θ is the current phase. If 0.6 ms is converted to current phase, it can be concluded that the hysteresis phase of AMF is less than 10.8° at power frequency. The ANSYS results for the AMF at IF current are shown in Fig. 5, where Q is the center point of the middle plane between the contacts and L is the diameter and the exciting current is 1 kA RMS in simulation. As the frequency is 400 Hz, the residual magnetic flux density of Q is 2.80 mT at CZ, and the hysteresis phase is about 20°. When the frequency is up to 800 Hz, the residual magnetic flux density of Q is 3.65 mT, and the hysteresis phase is much higher than 30°. This means that although with the increase of frequency, the delay time of AMF at IF is shorter than that of

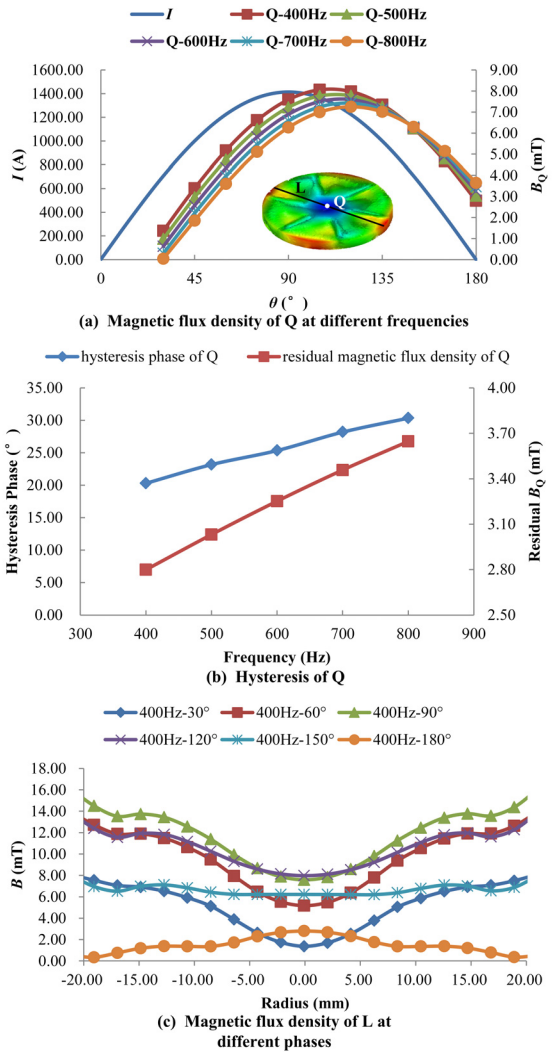

FIGURE 5. Magnetic flux density of Q and L.

the power frequency, the hysteresis phase, which arises due to the influence of frequency on AMF, is much larger than that of the power frequency. And from Fig. 5 (c), it can be seen that, before the current peak, the AMF of each point in L increases with the increase of current. However the increase rate of the center is slow and the B is lower than that of other regions. After the peak current, the further away from the center, the faster the AMF decreases. The change process also indicates that the magnetic field of the contact center is the most affected by the eddy current, and the hysteresis of AMF is the most obvious. Therefore, residual plasmas in arc gap will be under the control of residual magnetic field over a long phase and are difficult to spread quickly at IF, hindering the RRDS and hampering the arc reignition. Hence, the hysteresis of AMF is a very important factor determining the current interruption ability at IF.

C. POSITION OF ARC RECOGNITION

When interruption failed at 360 Hz and 22.4 kA, the arc reignition process in CuCr50 contacts is shown in Fig. 6 (a).

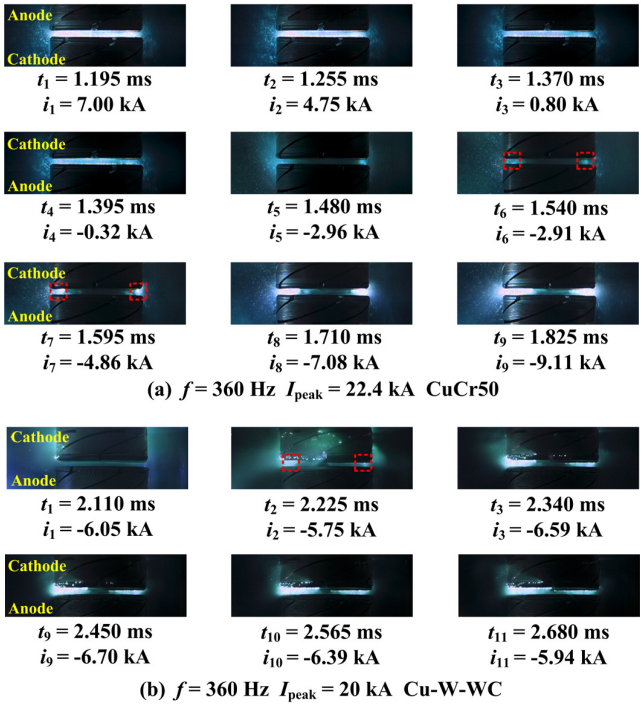

FIGURE 6. Arc reignition process in various contacts.

Before CZ, the upper contact is anode and the lower contact is cathode in the arc images from t_1 to t_3. Since t_4, the current decreases to zero and is inversed, then the old anode turns to be the new cathode and the old cathode turns to be the new anode. At t_6, it can be observed that the position of arc reignition is at the margin of the contacts. With the increase in current, the arc diameters expand and macroscopic particles sputter from the contacts in the process.

In the contact with various materials, such as Cu-W-WC, it can also be observed that reignition appeared on the contact margin first, as shown in Fig. 6 (b). Unlike the process CuCr50 contacts, There is no obvious particles at macroscopic level in the arc column. And there are not so many macroscopic particles; nevertheless some cathode spots appear around outside the new cathode. As the melting point of Cr is 1875°, and the melting points of W and WC are approximately 3000°, it is easier for metal evaporation and macroscopic particles to sputter from CuCr50 than from Cu-W-WC, and the ablation performance of CuCr50 is not as good as that of Cu-W-WC.

The input energy and the temperature of contact are high during the arc period. The diffusion rate of plasma is very high: about $1\sim2\times10^4$ m/s for the metal atoms and ions and 10^6 m/s for the electrons [19], which makes the diffusion time reach the microsecond level. However, for a metal contact with several thousand degrees centigrade after CZ, the cooling time must be much longer than the diffusion time of plasmas. Thus, in the high current mode, it is easy for electrons launching from the hot anode with high temperature, to be the new cathode and lead to arc reignition. Further, it can be seen

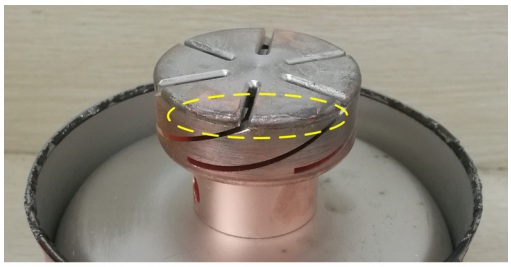

(a) Top view of the CuCr50 contacts

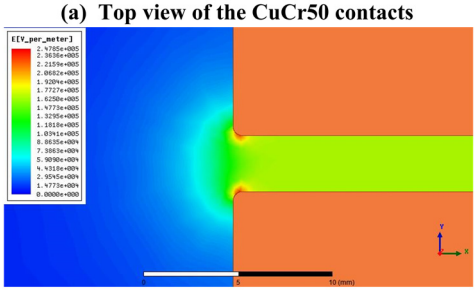

(b) Distribution of electric field in the contact distance

FIGURE 7. Ablation and electric field at the margin of the contact.

that, there are serious ablation areas at the margin after the experiment, as shown in the top view of the CuCr50 contacts in Fig. 7 (a).

Based on the experimental results, the maximum recovery voltage is about 500 V after CZ, when interruption failed. Then we apply a voltage difference between the contacts and calculate the distribution of electric field in the 3 mm distance, as shown in Fig. 7 (b), in which the electric field intensity is represented by color. The results show that the electric field intensity at the margin is twice as strong as that inside the contact because of the marginal effect, where the enhancement coefficient of electric field is 2.

According to the Fowler-Nordheim field emission theory, the relationship between current density and electric field intensity is given by [19]

$$\begin{cases} J = \dfrac{1.541 \times 10^{-2} E^2}{\varphi t^2(y)} \exp\left[\dfrac{-6.831 \times 10^9 \varphi^{3/2} v(y)}{E}\right] \\ y = \dfrac{3.795 \times 10^{-3} \sqrt{E}}{\varphi} \end{cases} \tag{8}$$

where J is the current density, E is the electric field intensity, φ is the work function and $t(y)$ and $v(y)$ are the field emission functions of Fowler-Nordheim. As expressed in equation (8), the current density is high where the electric field intensity is strong. Owing to the high current density, a large amount of metal vapor will be heated, melted and evaporated at the margin of the contact, thus increasing the probability of field emission. In addition, because of the strong electric field intensity, charged particles move faster and do not recombine easily at the marginal region. Due to the above reasons, the arc reignites first at the margin of the contact.

D. SPUTTERING OF MACROSCOPIC PARTICLES

The sputtering of macroscopic particles in CuCr50 contacts during reignition is captured by high-speed camera,

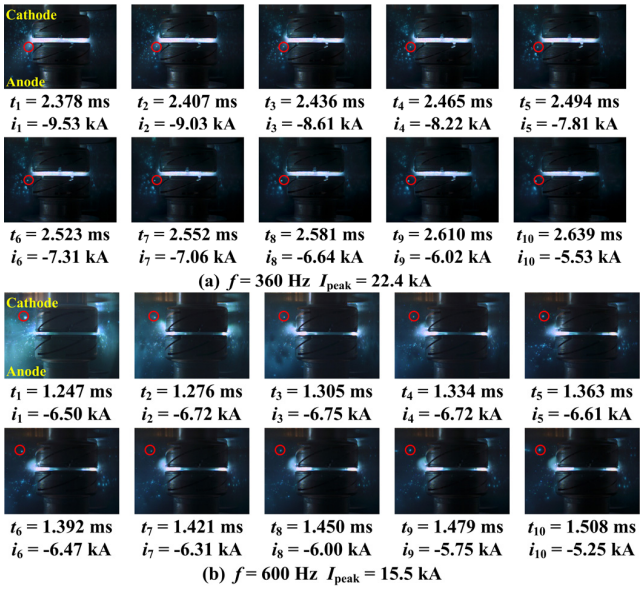

FIGURE 8. Sputtering of macroscopic particles in CuCr50 contacts during reignition.

as displayed in Fig. 8. Since the reignition, the upper contact is cathode and the lower contact is anode. It can be seen that there are many particles in the chamber and the sputtering is severe. We record 10 images continuously at each frequency and mark the observational particle by a red cycle.

By means of the frame differential method, the sputtering of marked particles is analyzed and the average velocity, vavg, the acceleration, a, and the angle, β, between the emission direction and the horizontal direction, are listed in TABLE 3.

TABLE 3. Parameters of macroscopic particles.

f [Hz]	v_{avg} [m/s]	a [m/s^2]	β [°]	$\bar{r}$ [mm]	m [mg]	F [mN]
360	10.86	10^5	13.24	0.55	5.50	550.28
500	19.04	1.2×10^5	13.40	0.41	2.28	273.54
600	19.44	1.4×10^5	24.30	0.68	10.40	1455.96

The macroscopic particles sputtering is driven by the pressure inside the arc area, as illustrated in Figure 9.

According to our previous research [20], if the pressure gradient is considered to be constant along the emission direction, which is $\boldsymbol{w}$, the pressure gradient in arc area will be related to the acceleration. Further, referring to the average radius, r of particles, the mass of the macroscopic particles which is m, and the force which is F in the pressure field, can be calculated by

$$\begin{cases} \dfrac{\partial P}{\partial w} = \rho a \\ F = \displaystyle\int \mathrm{d}F = \frac{4}{3}\pi r^3 \frac{\partial P}{\partial w} \end{cases} \tag{9}$$

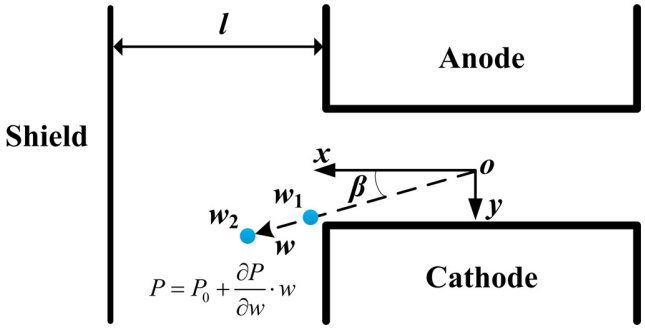

FIGURE 9. Pressure of macroscopic particles sputtering process.

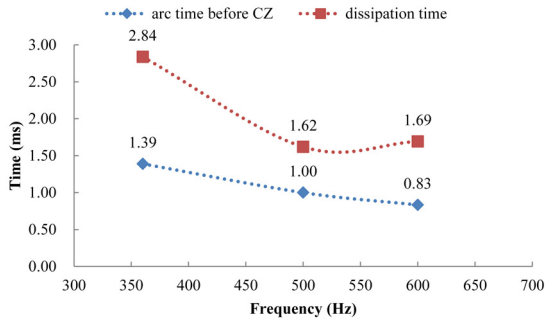

FIGURE 10. Dissipation time of the macroscopic particles at different frequencies.

In addition, the macroscopic particles would not disappear until they reach the inner surface of the shield cover, and the particles will be solidified. The dissipation time is associated with the average velocity and the emission angle, as expressed by

$$t = \frac{l}{\cos\beta \cdot v_{\text{avg}}} \tag{10}$$

The calculated results are shown in Fig. 10.

Before CZ, the half cycle time is the arc time. The dissipation time, which involves particle moving and being solidified after CZ, of the macroscopic particles will be longer than the arc time before CZ at various frequencies. Thus, the arc reignition is impacted by the macroscopic particles sputtering, which may be the source of plasmas and metal vapors post arc. If the density of particles and metal vapors are large enough, the arc will reignite by breakdown.

IV. CONCLUSIONS

Based on the experimental results and analysis, we have drawn the following conclusions, which would be beneficial to the parameters design of IF vacuum circuit breakers, such as the magnetic flux density of AMF, chamfering of contact margin and contact materials.

(1) With the increase of frequency, the current interruption ability of AMF vacuum circuit breaker decreases from 22.4 kA at 360 Hz to 14.0 kA at 850 Hz. On one hand, the rate of change of current, di/dt, at CZ reaches the breaking threshold at a smaller current value with higher frequency. Based on the least squares solution of the Mayr model, the time of decay of arc energy is prolonged when interruption fails, which is disadvantageous to the breaking process. On the other hand, the eddy effect is enhanced at higher frequency, which increases the residual magnetic induction intensity and hysteresis phase of AMF after CZ. As a result, the diffusion of plasma is blocked.

(2) In the experiments on contacts with various materials, we observed that the position of arc reignition always appears at the margin of contacts. It is shown by calculation that the electric field at the marginal area is twice as strong as that inside the contact. The current density is high where the electric field is strong, leading to higher probability of field emission.

(3) Arc images are analyzed by frame differential method. The sputtering velocity of macroscopic particles is estimated to be 10-20 m/s. The dissipation time of the macroscopic particles is longer than the arc time of IF vacuum arc, and the presence of macroscopic particles seems to lead to the arc reignition.

REFERENCES

[1] J. Wang, J. Wu, and L. Zhu, "Properties of intermediate-frequency vacuum arc under axial magnetic field," *IEEE Trans. Plasma Sci.*, vol. 37, no. 8, pp. 1477–1483, Aug. 2009. [Online]. Available: http://ieeexplore.ieee.org/document/5175466/

[2] J. Wang, J. Wu, and L. Zhu, "Arc behavior of intermediate-frequency vacuum arc on axial magnetic field contacts," *IEEE Trans. Plasma Sci.*, vol. 39, no. 6, pp. 1336–1343, Jun. 2011. [Online]. Available: http://ieeexplore.ieee.org/document/5756249/

[3] Z. Liying, W. Jianwen, and Z. Xueming, "Arc movement of intermediate-frequency vacuum arc on TMF contacts," *IEEE Trans. Power Del.*, vol. 28, no. 4, pp. 2014–2021, Oct. 2013. [Online]. Available: http://ieeexplore.ieee.org/document/6570744/

[4] L. Zhu, J. Wu, B. Liu, and Y. Feng, "The dynamic volt-ampere characteristics of a vacuum arc at intermediate-frequency under a transverse magnetic field," *Plasma Sci. Technol.*, vol. 15, no. 1, pp. 30–36, Jan. 2013. [Online]. Available: http://iopscience.iop.org/article/10.1088/1009-0630/15/1/06/meta

[5] L. Zhu, J. Wu, and Y. Jiang, "Motion and splitting of vacuum arc column in transverse magnetic field contacts at intermediate—Frequency," *Plasma Sci. Technol.*, vol. 16, no. 5, pp. 454–459, May 2014. [Online]. Available: http://iopscience.iop.org/article/10.1088/1009-0630/16/5/03/meta

[6] Y. Jiang and J. Wu, "Interruption phenomenon in intermediate-frequency vacuum arc," *Plasma Sci. Technol.*, vol. 18, no. 3, pp. 311–318, Mar. 2016. [Online]. Available: http://iopscience.iop.org/article/10.1088/1009-0630/18/3/16/meta

[7] E. Schade and E. Dullni, "Recovery of breakdown strength of a vacuum interrupter after extinction of high currents," *IEEE Trans. Dielectr. Electr. Insul.*, vol. 9, no. 2, pp. 207–215, Apr. 2002. [Online]. Available: http://ieeexplore.ieee.org/document/993737/

[8] J. V. R. Heberlein and J. G. Gorman, "The high current metal vapor arc column between separating electrodes," *IEEE Trans. Plasma Sci.*, vol. PS-8, no. 4, pp. 283–288, Dec. 1980. [Online]. Available: http://ieeexplore.ieee.org/document/4317328/

[9] H. C. Miller, "Anode modes in vacuum arcs," *IEEE Trans. Dielectrics Electr. Insul.*, vol. 4, no. 4, pp. 382–388, Aug. 1997. [Online]. Available: http://ieeexplore.ieee.org/document/625352/

[10] R. Gilles, K.-D. Weltmann, E. Schade, and M. Claessens, "Numerical simulation of the residual charge of vacuum interrupters," *IEEE Trans. Plasma Sci.*, 2001, vol. 29, no. 5, pp. 754–758, Oct. 2001. [Online]. Available: http://ieeexplore.ieee.org/document/964469/

[11] B. Gellert, "Measurement of high copper vapour densities by laser-induced fluorescence," *J. Phys. D, Appl. Phys.*, vol. 21, no. 5, pp. 710–717, 1988. [Online]. Available: http://iopscience.iop.org/article/10.1088/0022-3727/21/5/007

[12] Y.-M. Sung, Y. Zhu, M. Otsubo, and C. Honda, "Spatio-temporal distributions of copper vapor particles in a vacuum arc discharge plasma," *IEEE Trans. Plasma Sci.*, vol. 33, no. 5, pp. 1491–1496, Oct. 2005. [Online]. Available: http://ieeexplore.ieee.org/document/1518967/

[13] K. Watanabe *et al.*, "The anode surface temperature of CuCr contacts at the limit of current interruption," *IEEE Trans. Plasma Sci.*, vol. 25, no. 4, pp. 637–641, Aug. 1997. [Online]. Available: http://ieeexplore.ieee.org/document/640677/

[14] S. Jia, D. Yang, L. Wang, and Z. Shi, "Investigation of the swirl flow on anode surface in high-current vacuum arcs," *J. Appl. Phys.*, vol. 111, no. 4, p. 043301, Feb. 2012. [Online]. Available: http://aip.scitation.org/doi/10.1063/1.3684974

[15] D. Yang, L. Wang, S. Jia, L. Wang, Z. Shi, and Y. Li, "Experimental investigation of anode activities in high-current vacuum arcs," *IEEE Trans. Plasma Sci.*, vol. 38, no. 2, pp. 206–213, Feb. 2010. [Online]. Available: http://ieeexplore.ieee.org/document/5378621/

[16] T. Qin, E. Dong, G. Liu, and J. Zou, "Recovery of dielectric strength after DC interruption in vacuum," *IEEE Trans. Dielectr. Electr. Insul.*, vol. 23, no. 1, pp. 29–34, Feb. 2016. [Online]. Available: http://ieeexplore.ieee.org/document/7422542/

[17] J. Onuki, Y. Anazawa, M. Nihei, M. Katou, A. Onuma, and T. Funamoto, "Development of a new high-frequency, high-peak current power source for high constricted arc formation," *Jpn. J. Appl. Phys.*, vol. 41, no. 9, pp. 5821–5826, Sep. 2002. [Online]. Available: http://iopscience.iop.org/article/10.1143/JJAP.41.5821/meta

[18] Z. Wang, Y. Zheng, Z. Liu, and S. Cheng, "Arc behaviours in vacuum interrupters with axial magnetic field electrodes," *Plasma Sci. Technol.*, vol. 10, no. 5, pp. 569–574, 2008, May. [Online]. Available: http://iopscience.iop.org/article/10.1088/1009-0630/10/5/10

[19] J. M. Lafferty, *Vacuum Arc: Theory and Application*. New York, NY, USA: Wiley, 1979, pp. 26–38.

[20] Y. Jiang, J. Wu, M. Chen, and W. Huo, "Analysis of the vacuum arc interruption process in aviation intermediate-frequency power supply systems," *Energies*, vol. 10, no. 3, p. 353, Mar. 2017. [Online]. Available: http://www.mdpi.com/1996-1073/10/3/353

JIANG YUAN (M'17) was born in Dandong, China, in 1985. He received the B.S. and M.S. degrees in materials science and engineering and the Ph.D. degree in electrical engineering from Beihang University, Beijing, China, in 2008, 2011, and 2016, respectively.

From 2016 to 2017, he was with China North Industries Group Corporation. He is currently a Post-Doctoral Fellow at Beihang University. His research interests include the theory and application of vacuum arcs and the control of intelligent electrical apparatuses.

WU JIANWEN (M'15) received the B.S. and M.S. degrees in electrical engineering from the Shenyang University of Technology, Shenyang, China, in 1984 and 1987, respectively, and the Ph.D. degree in electrical engineering from Xi'an Jiaotong University, Xi'an, China, in 1995.

From 1995 to 1998, he was a Post-Doctoral Fellow at the Huazhong University of Science and Technology, Wuhan, China. Since 2001, he has been a member of the Faculty of the School of Automation Science and Electrical Engineering, Beijing, China, where he is currently a Professor. His research interests include the theory of vacuum arcs, intelligent electrical apparatuses, and power electronics technology.

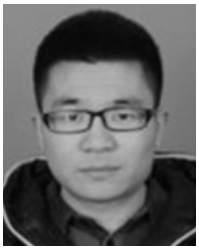

JIA BOWEN was born in Beijing, China, in 1992. He received the M.S. degree in electrical engineering from Beihang University, Beijing, China, in 2017, where he is currently pursuing the Ph.D. degree in electric machines and electric apparatus.

His research interests include plasma characteristics and the mechanism of dc arc interruption in hydrogen and mixed gases, the design of high powered dc relays, and dc breaker technology.